

Megamaser detection and nuclear obscuration in Seyfert galaxies

Michael Ramolla¹, Martin Haas¹, Vardha Nicola Bennert², and Rolf Chini^{1,3}

¹ Astronomisches Institut, Ruhr-Universität Bochum, Universitätsstraße 150, 44801 Bochum, Germany

² Department of Physics, University of California, Santa Barbara, CA 93106, USA

³ Facultad de Ciencias, Universidad Católica del Norte, Antofagasta, Chile

Received June 21, 2010; accepted February 10, 2011

ABSTRACT

We revisit the relation between H₂O maser detection rate and nuclear obscuration for a sample of 114 Seyfert galaxies, drawn from the CfA, 12 μ m and IRAS F25/F60 catalogs. These sources have mid-infrared spectra from the Spitzer Space Telescope and they are searched for X-ray and [O III] 5007Å fluxes from the literature. We use the strength of the [O IV] 25.9 μ m emission line as tracer for the intrinsic AGN strength. After normalization by [O IV] the observed X-ray flux provides information about X-ray absorption. The distribution of X-ray / [O IV] flux ratios is significantly different for masers and non-masers: The maser detected Seyfert-2s (Sy 1.8-2.0) populate a distinct X-ray / [O IV] range which is, on average, about a factor four lower than the range of Seyfert-2 non-masers and about a factor of ten lower than the range of Seyfert-1s (Sy 1.0-1.5). Non-masers are almost equally distributed over the entire X-ray / [O IV] range. This provides evidence that high nuclear obscuration plays a crucial role for the probability of maser detection. Furthermore, after normalization with [O IV], we find a similar but weaker trend for the distribution of the maser detection rate with the absorption of the 7 μ m dust continuum. This suggests that the obscuration of the 7 μ m continuum occurs on larger spatial scales than that of the X-rays. Hence, in the AGN unified model, at moderate deviation from edge-on, the 7 μ m dust absorption may occur without proportionate X-ray absorption. The absorption of [O III] appears unrelated to maser detections. The failure to detect masers in obscured AGN is most likely due to insufficient observational sensitivity.

Key words. Galaxies: Seyfert – Galaxies: nuclei – Masers – X-rays: galaxies – Infrared: galaxies

1. Introduction

H₂O megamaser galaxies represent an extreme subclass of active galactic nuclei (AGN) with strong water maser emission at 22 GHz (reviews by Lo 2005 and Henkel et al. 2005). In those cases where the emission arises from a molecular disk and can be resolved spatially using Very Long Baseline Interferometry, the central black hole (BH) mass and the distance to the galaxy can be determined (e.g. for NGC 4258, Greenhill et al. 1993, Herrnstein et al. 1999). Thus, finding megamasers (*henceforth simply called masers*) and understanding their properties is of great interest.

From theoretical considerations, a large line-of-sight column density of velocity coherent gas favors the detection of a maser. High velocity coherence of the maser emitting gas is required, because energy and momentum conservation imply that the induced photon has the same frequency and direction as the stimulating photon (e.g. Elitzur 2002). While the emission of an individual maser spot is directional (i.e. beamed), a collection of such spots statistically may be expected to radiate in all directions, but this has not been confirmed so far. The originally discovered water maser emission from AGN comes from (presumably edge-on) disks, and the resolved emission in most sources traces accretion disks while a few cases are star formation masers. However, two sources, Circinus and NGC 3079, show in addition also off-disk jet masers that seem to trace outflows. Potentially these outflow masers are actually torus clouds (Nenkova et al. 2008).

In the AGN unified model, an optically thick obscuring dust torus is envisioned to encircle the accretion disk and type-1 AGN are seen pole-on while type-2 AGN are seen edge-on (Antonucci

1993). Masers are almost exclusively found in AGN of Seyfert-2 or LINER type, consistent with the picture that masers are preferentially beamed in the plane of the torus (Braatz et al. 1997, 2004, Henkel et al. 2005). But not all type-2 AGN are masers.

From the conceptional viewpoint, it should be noted that the 22GHz radio-frequency maser emission itself is believed to be largely unaffected by absorption; but a high X-ray, optical or mid-infrared obscuration may signpost a high likelihood that the masing disk is seen edge-on, hence favoring a maser detection.

Type-2 AGN that host masers show a prevalence (> 80%) of high X-ray obscuring columns ($N_H > 10^{23}\text{cm}^{-2}$) and about half are Compton thick ($N_H > 10^{24}\text{cm}^{-2}$) (Braatz et al. 1997, Zhang et al. 2006, Greenhill et al. 2008). However, as pointed out by Zhang et al. (2006), among type-2 AGN the average X-ray derived column densities of masers and non-masers¹ are indistinguishable. One explanation for this unexpected result could be that X-ray scattering in clumpy media dilutes the true line-of-sight column density, and thus prevents us from deriving unbiased orientation information. Therefore it is vital to include also information from other than X-ray wavelengths, to reveal the potential influence of nuclear obscuration on the maser detection and non-detection, respectively.

Recently, Zhang et al. (2010) analyzed the K α iron line equivalent width EW(K α), following the strategy of Bassani et al. (1999), and compared it with two optical thickness parameters, the infrared 6-400 μ m luminosity L_{IR} derived from IRAS 12-100 μ m photometry and the [O III] 5007Å emission line luminosity $L_{[\text{O III}]}$. Both parameters were adopted to

¹ We denote as non-masers those AGN that have been observed at 22 GHz, but for which no megamaser was detected.

be isotropic tracers for the intrinsic AGN strength. While the $EW(K\alpha)$ distributions of 19 masers and 34 non-masers cover the same broad range (100 - 3000 eV), the median $EW(K\alpha)$ of masers is about a factor 4 higher than that of the non-masers, indicating that the X-ray continuum of masers is more absorbed than that of non-masers.

However it is still a matter of debate, whether L_{IR} and $L_{[OIII]}$ are indeed isotropic tracers of the intrinsic AGN luminosity. While [O III] has often been used as isotropic AGN tracer (Mulchaey et al. 1994; Alonso-Herrero et al. 1997; Bassani et al. 1999; Heckman et al. 2005; Panessa et al. 2006; Lamastra et al. 2009), the discovery of polarized [O III] emission in some type-2 AGN (di Serego Alighieri et al. 1997) cautions that a substantial fraction of [O III] can be shielded by the torus. Further studies, using MIR emission lines like [O IV] or [Ne V] as orientation independent tracer of the AGN power, provide evidence by means of the [O III]/[O IV] ratio, that [O III] suffers orientation dependent extinction, up to a factor of 10 in individual cases (Haas et al. 2005, Meléndez et al. 2008a, Baum et al. 2010).

This is qualitatively consistent with results obtained using the (extinction corrected) 2-10keV X-ray luminosity L_X as intrinsic AGN power measure; Netzer et al. (2006) find that $L_{[OIII]}/L_X$ of type-2 AGN is, on average, about a factor two lower than that of type-1 AGN. From a conceptional viewpoint, even in the face-on Sy1 case, the back-sided cone of the NLR lies – at least partly – behind an absorbing layer (e.g. the dust torus). Therefore it is highly questionable how far [O III] can serve as an isotropic AGN tracer. The extinction correction via Balmer decrement ($H_\alpha/H_\beta = 3$) remains highly uncertain, since it is dependent on the geometry of the emitting and obscuring regions.

Hes et al. (1996); Baker (1997) caution against the use of [O III] as a measure of the intrinsic NLR emission and suggest to use [O II] 3727 instead. Observations of radio-loud AGN, where the orientation can be inferred from radio morphology, show that [O II] is largely orientation independent (Hes et al. 1996; Baker 1997). On the other hand, because of its low ionization potential, [O II] can also be dominated by star formation in the host (e.g. Ho 2005). Then, the decline of $L_{[OII]}/L_X$ with increasing L_X , as found by Netzer et al. (2006), could be naturally explained by a decline of host/AGN with increasing AGN L_X .

Likewise the mid-infrared ($\lambda < 40\mu m$) part of L_{IR} is orientation dependent (e.g. Fig. 16 in Buchanan et al. 2006), while the far-infrared ($\lambda > 40\mu m$) emission of Seyfert galaxies and low-luminosity quasars actually is dominated by star forming contributions rather than by the AGN itself (e.g. Maiolino & Rieke 1995, Schweitzer et al. 2006). Thus, a careful re-investigation using more suited isotropic AGN tracers would be desirable.

Here, we revisit the connection between maser detection rate and nuclear obscuration using the strength of the [O IV] $25.9\mu m$ emission line (for short [O IV]) as tracer for the intrinsic AGN strength. [O IV] has been found to be largely unaffected by obscuration (e.g., Genzel et al. 1998, Haas et al. 2005, Meléndez et al. 2008a, Baum et al. 2010). We combine the strategies of Bassani et al. (1999) and Meléndez et al. (2008a). The observed X-ray (2-10 keV) flux normalized by [O IV] should provide information about X-ray absorption, even in the case of X-ray scattering caused by a complex geometry or for Compton thick cases. We compare the distribution of X-ray / [O IV] for masers and non-masers. In addition, after normalization with [O IV], we inspect the relation between maser detection rate and absorption of the $7\mu m$ dust continuum emitted from the nuclear torus, as well as maser detection and the

absorption of the [O III] 5007\AA emission of the central part of the narrow-line-region (NLR).

The distances from which we derived the luminosities are taken from the NED database. The cosmology is based on $H_0 = 73 \text{ km s}^{-1} \text{ Mpc}^{-1}$, $\Omega_\Lambda = 0.73$ and $\Omega_m = 0.27$.

2. Data

2.1. The parent sample

At first glance, one could take all known masers and non-masers from the literature and compare their properties, for instance $L_X/L_{[OIV]}$. But in order to determine nuclear obscuration, one needs to know also the range of $L_X/L_{[OIV]}$ for unobscured (preferentially Sy1) sources, which should comprise a complete sample free from any selection bias. However, the list of Seyferts, for which a maser search has been performed, did not follow clear selection criteria. Even worse, most maser searches have been performed on Sy2s, but only a small number on Sy1s. Because incomplete sample selection may influence the results, we here decided to start with complete Seyfert catalogs having well defined selection criteria. In order to increase the sample size, we created a master sample from the following three catalogs, consisting of a total of 163 sources.

- The magnitude limited complete sample of the CfA Redshift Survey by Huchra & Burg (1992), which was supplied with updated Seyfert-type information from the NED database.
- The $12\mu m$ Active Galaxy Sample by Spinoglio & Malkan (1989), complemented by Rush & Malkan (1993).
- The IRAS F25/F60 flux-ratio selected sample by de Grijp et al. (1992), as refined by Schmitt et al. (2003).

Table 1 documents how the 163 sources distribute over the three catalogs, and how these catalogs match or complement each other. In general, we will present the results for the combined sample, but – where necessary – also for the catalogs individually (Tab. 2).

Further below (Section 3.4) we will discuss potential differences between the three samples and our combined sample and all other known masers outside of it. The Spitzer data archive contains IRS spectra (at $\sim 26\mu m$) for 126 of the 163 sources classified as Seyferts according to the NED. This data is listed in Tab. 3. It covers the complete CfA-sample of 54 Seyfert Galaxies. It includes 107 of 118 Seyferts (two Blazars included as Sy1) from the $12\mu m$ selected sample. For the IRAS sample we found useful IRS spectra for 34 of 60 sources.

2.2. Maser information

The parent sample of 126 sources with Spitzer spectra was searched for known maser-detections and non-detections. For this purpose we used the lists as compiled by Bennert et al. (2009) and on the website of the Hubble Constant Maser Experiment (HoME)².

This search results in 18 masers (3 Sy1s, 15 Sy2s), 96 non-masers (36 Sy1s, 60 Sy2s) and 12 sources (10 Sy1s, 2 Sy2s) for

² <http://www.cfa.harvard.edu/~lincoln/demo/HoME/surveys/survey.html>
compiled from Kondratko et al. (2006b,a); Hagiwara et al. (2003); Zhang et al. (2006); Braatz et al. (2004); Hagiwara et al. (2002); Greenhill et al. (2002, 1997); Sato et al. (2005); Braatz et al. (1996); Greenhill et al. (1995); Nakai et al. (1995); Henkel et al. (1998, 2005); Braatz et al. (2003); Henkel et al. (1984); Haschick & Baan (1985); Claussen & Lo (1986); Henkel et al. (1986); Becker et al. (1993); Greenhill et al. (1990); Braatz & Gugliucci (2008); Henkel (2008); Braatz (2008)

which no maser search has been performed so far (henceforth called maser-unknown). The results are listed in Tab. 3, Col. 2.

2.3. [O IV] 25.89 μm Line and 7 μm Continuum Flux

Our analysis is based on public archival IRS spectra of Seyfert galaxies. We used the post-basic-calibration data (PBCD), as reduced by the Spitzer Science Center's (SSC) pipeline. This included droop-, stray-light-, cross-talk- and saturation correction, dark subtraction, flatfielding and coaddition.

If possible, the IRS high resolution spectra with $R \sim 600$ have been chosen, to avoid contamination of [O IV]_{25.89 μm} with the neighboring [Fe II]_{25.99 μm} emission line. If high-resolution spectra were not available, the low-resolution spectra were used, including a background subtraction, which was also performed by the SSC pipeline.

For the high resolution data, collected with the shorter (4.7 x 11.3 and 11.1 x 22.3 arcsec) slits, separate background observations had to be chosen to evaluate the background contribution. This was performed in Ramolla (2009), by comparing the background with the source fluxes at the presumably weakest part of the source spectrum between 9 and 10 μm rest frame; with the result that the background contribution is negligible in comparison with the conservatively assumed flux calibration errors of 15%. The resulting errors are calculated from an assumed 15% flux calibration error and the error of the line fitting routine.

The [O IV] flux has been extracted by fitting a simple spectral model in a wavelength-window of $\sim 0.3 \mu\text{m}$ around the [O IV] line. This model consists of a linear base, convolved with Gaussian profiles that also include the neighboring [Fe II] line. No [O IV] aperture corrections had to be applied, because for both, high- and low-resolution data, the slit apertures cover an area larger than the expected size of the NLR, as estimated from the relationship³ of [O III] luminosity to NLR size, found by Bennert et al. (2002).

We calculated the 7.6 μm (henceforth for short 7 μm) continuum flux from the background-subtracted IRS low-resolution spectra. We used a modified version of the PAHFIT code by Smith et al. (2007) which estimated the continuum in the 5 to 11.8 μm branch. As suggested by Smith & Draine (2008), we did not correct the continuum fit for the silicate feature at 9.7 μm . The 7 μm continuum flux is then calculated from the PAH flux and the equivalent-width of the features at 7.4 μm , 7.6 μm and 7.8 μm (Ramolla 2009). The uncertainties of the 7 μm continuum are conservatively estimated to be smaller than 30%, which is sufficient for our purpose. In a few cases the AGN contribution may be contaminated by nuclear ($<3.7''$) star formation (e.g. Deo et al. 2009). We checked that the effect on our statistical analysis is negligible by comparison with high resolution ground-based MIR observations.

The [O IV] and 7 μm fluxes are listed in Tab. 3. The values are consistent with those derived by others (Buchanan et al. 2006, Deo et al. 2007, Deo et al. 2009, Tommasin et al. 2010).

2.4. X-rays + [O III] 5007 Å line from the literature

The 2-10 keV hard X-Ray data have been obtained by several observers using ASCA, Beppo SAX, Chandra and XMM. We collected the data from the NED; in case of multiple entries we chose the latest detection.

We have collected [O III] 5007 Å emission line fluxes from various literature sources, as listed in Tab. 3. Because of the

large uncertainties, we did neither apply any extinction correction nor any aperture correction for the [O III] fluxes. Such aperture corrections would affect a few very nearby sources, but most sources are sufficiently distant so that in the statistical analysis any bias is small.

2.5. Additional maser sources

On the one hand, our combined sample is drawn from the CfA, 12 μm and IRAS F25/F60 catalogs, containing 15 Sy2 maser sources with Spitzer spectra. On the other hand a total of 52 masing Sy2 are known so far (Bennert et al. 2009; Zhang et al. 2010), although drawn from different AGN catalogs using inhomogeneous criteria.

In order to compare the 15 Sy2 maser of our combined sample with the remaining 37, we also analyzed available Spitzer spectra and gathered further [O III] and X-ray fluxes for them from the literature in the same manner, as we did on our combined sample. This results in an "off-sample" list of 37 Sy2 masers that is appended to Tab. 3.

3. Results and discussion

While our combined sample of 126 sources contains 114 maser and non-maser sources (12 maser-unknown excluded), not all of them have data in all observables considered here (X-rays, $F_{7\mu\text{m}}$, [O III]). Therefore, we compare the maximum possible subsets for pairs of observables, and discuss the implications in the framework of the AGN unified model. Therein we consider as components the accretion disk, supposed to house the maser, the dust torus, the bi-conical NLR and the host galaxy. We here denote by Sy1s the subtypes between Seyfert 1.0 and 1.5, and by Sy2s those between Seyfert 1.8 and 2.0. All Figures contain an combined error bar in the lower right corner that is averaged from all relative errors in this measure. Since the literature sources did not uniformly presented errors, we do not perform this step for the X-ray, [O III] and H₂O luminosities.

3.1. Nuclear X-ray obscuration

Figure 1 shows the observed hard X-ray versus [O IV] line luminosities, and Figure 2 the $L_X/L_{[\text{O IV}]}$ histogram. The features are:

- On average, Sy1s present an about 10 times higher X-ray/[O IV] ratio than Sy2s.
- Sy2 non-masers are evenly distributed over the entire range occupied by Sy2 masers and by Sy1s (Fig. 1).
- Sy2 masers are almost disjoint from Sy1s. At a given [O IV] luminosity, Sy2 masers have on average about a factor 4 lower X-ray luminosity than Sy2 non-masers (Fig. 2). Likewise, the few Sy1 masers have a lower X-ray luminosity than Sy1 non-masers.⁴
- 6 out of 12 sources without masing information, but L_X and $L_{[\text{O IV}]}$ available (see Tab. 3), show the same trends as the Sy1s and Sy2s with masing information (see Tab. 2). They are not plotted, to avoid overcrowding of Figs. 1 and 2 with too many different symbols.

⁴ The Sy1 masers are NGC 4051, NGC 4151 and UCG 5101. Note that both NGC 4051 and NGC 4151 have relatively low maser H₂O luminosity, and UCG 5101 is an ultra-luminous infrared galaxy so that the maser luminosity could arise from starburst regions rather than from the AGN accretion disk.

³ $\log(R_{\text{NLR}}) = (0.52 \pm 0.06) \times \log(L_{[\text{O III}]}) - (18.5 \pm 2.6)$

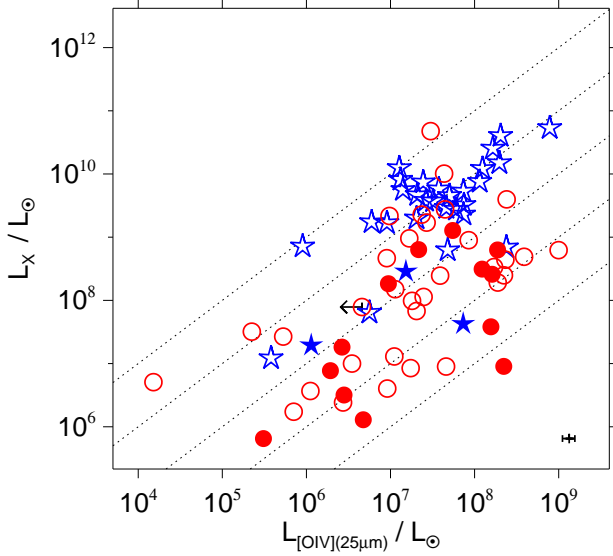


Fig. 1. Observed 2-10 keV X-ray versus [OIV] line luminosity. Blue stars represent Sy1s (Sy 1.0-1.5), red circles Sy2s (Sy 1.8-2.0). Filled symbols are masers, open symbols are non-masers. The dotted lines mark fixed $L_X/L_{[OIV]}$ ratios of 1000; 100; 10; 1; 0.1 (from top to bottom). The error-bar in the lower right corner is the average relative error of all [OIV] measurements.

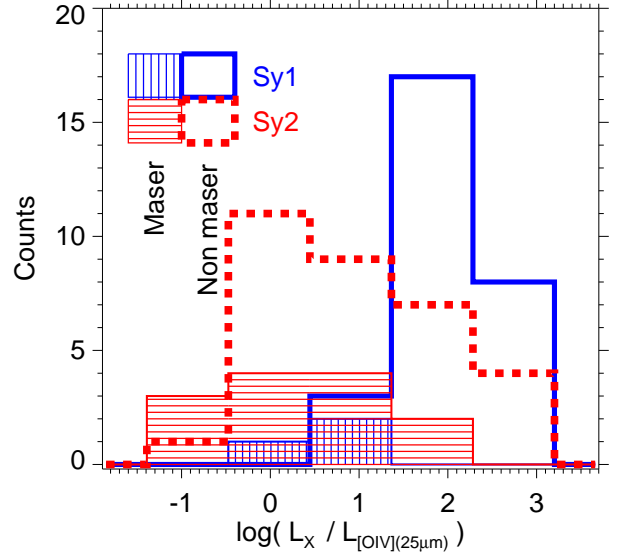


Fig. 2. Histogram of the $L_X/L_{[OIV]}$ ratio of the data points shown in Fig. 1. The red dashed line represents Sy2 non-masers, whereas the blue thick line represents the Sy1 non-masers. The maser-detections are represented by the dashed surfaces - blue and vertically dashed for Sy1, red and horizontally dashed for Sy2. The one upper limit is excluded.

We assume that the X-ray deficit, i.e. the decrease of $L_X/L_{[OIV]}$, is caused by obscuration, probably in the molecular dust torus. Then, the Figures 1 and 2 clearly demonstrate that masers are found almost exclusively in Sy2s with heavy nuclear obscuration, while non-maser Sy2s exhibit a broad range of X-ray absorption. A two-sided Kolmogorov-Smirnov (KS) test, applied on the $L_X/L_{[OIV]}$ distribution, results in a probability of 18% that the Sy2 masers and non-masers are drawn from the same parent population. Our results agree with those of Greenhill et al. (2008) and Zhang et al. (2010) who find that about 60% of the masers are Compton-thick.

Assuming that Sy1s are almost unobscured, the obscured sources populate the $L_X/L_{[OIV]}$ range below 10 in Fig. 1. Thus, masers populate almost completely the range of obscured sources. Surprisingly this range also contains numerous non-masers. In order to better understand why in such absorbed sources the maser search failed, we consider the influence of observed brightness. Fig. 3 shows the X-ray and [OIV] flux distribution (instead of the luminosity distribution). In fact, the Sy2 masers and non-masers show a flux-dependence in their [OIV] distribution. Sources with low [OIV] flux are more frequently classified as non-masers (2 Sy2 maser and 12 Sy2 non-maser at $L_{[OIV]} < 10^{-16} \text{ W m}^{-2}$), while sources with high [OIV] flux are more frequently classified as masers (6 Sy2 maser and 5 Sy2 non-maser at $L_{[OIV]} > 10^{-15} \text{ W m}^{-2}$). Fig. 4 displays the [OIV] fluxes of all Sy2s lying below the dividing line between obscured and unobscured sources ($L_X : L_{[OIV]} \approx 10$). Among this subset of obscured Sy2s, the frequency of non-masers rises constantly towards lower [OIV] fluxes, in contrast to the distribution of masers. This incidence is consistent with an observational bias against the maser-detection for faint AGN. This implies a relation between [OIV] flux and H_2O flux which is indeed observed in Fig. 9 and discussed in Section 3.5.

Because the detection of maser emission appears to be biased against sources with low flux, we conclude that among obscured

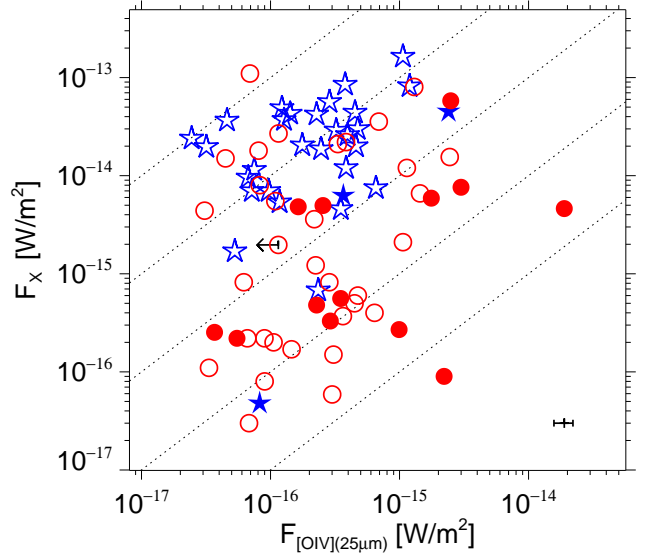


Fig. 3. Observed X-ray versus [OIV] line flux. Symbols and colors are as in Fig. 1. The dotted lines mark fixed flux ratios of 1000; 100; 10; 1; 0.1 (from top to bottom). The error-bar in the lower right corner is the average relative error of all [OIV] measurements.

sources the true fraction of masers is higher than indicated by Fig. 2.

3.2. Extended obscuration of the dust torus and the NLR

Figure 5 shows a histogram of the MIR $7 \mu\text{m}$ continuum to [OIV] line ratio. The striking features of this diagram are:

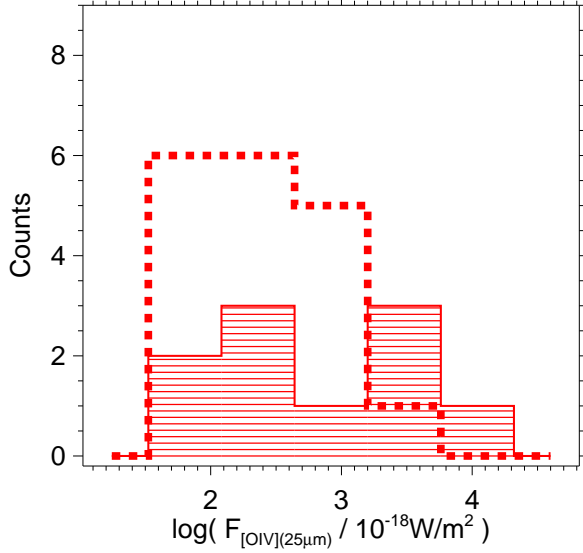


Fig. 4. [O IV] flux histogram of Sy2 masers for absorbed sources from Fig. 3 with $L_X / L_{[\text{OIV}]}$ < 10. Masers are represented by the shaded area, non-masers by the thick dashed histogram.

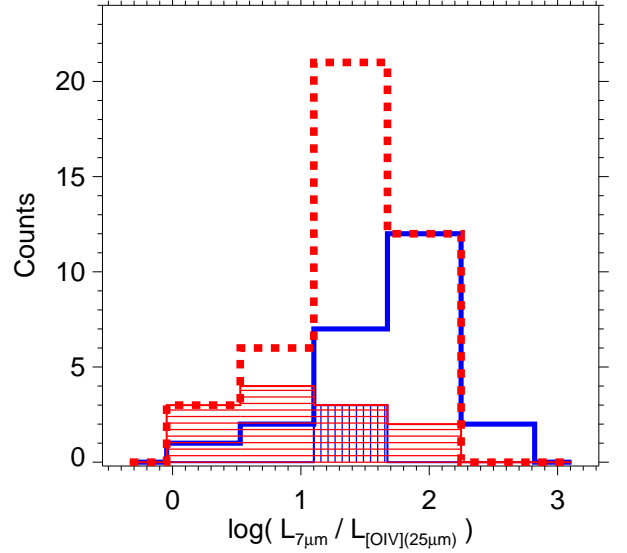


Fig. 5. Histogram of the $7\mu\text{m}$ continuum to [O IV] line ratio. Legend as in Fig. 2. All 21 upper limits from Tab. 3 are excluded.

- Sy2s populate about the same total range as Sy1s, but show a prevalence for lower $7\mu\text{m} / [\text{OIV}]$ values, i.e. a $7\mu\text{m}$ continuum deficit. On average, the ratio $7\mu\text{m} / [\text{OIV}]$ of Sy2s is about a factor of 3 lower than that of Sy1s. This is consistent with the results obtained via radio normalization ($7\mu\text{m} / 8\text{GHz}$) by Buchanan et al. (2006, their Fig. 16).
- Among Sy2s the $7\mu\text{m} / [\text{OIV}]$ ratio of masers is, on average, about a factor of 2 lower than that of non-masers. A KS test results in a probability of 3.7% that the Sy2 masers and non-masers are drawn from the same parent distribution. Flux considerations similar to those for $L_X / L_{[\text{OIV}]}$ suggest that the true $7\mu\text{m} / [\text{OIV}]$ separation of masers and non-masers will be even more pronounced once the observational bias against the detection of low flux masers is taken into account.

We assume that the deficit of the $7\mu\text{m}$ continuum in Sy2s is mainly caused by absorption of the torus dust emission. This absorption has to take place somewhere between the emitting region and the observer, hence probably in the "halo" of the torus, i.e. in the outer part of the torus itself or in the host galaxy. It is possible that the scale height of this MIR-absorbing halo, i.e. the projected distance of absorbing material from the line-of-sight to the nuclear accretion disk, is (much) larger than the scale height of the torus itself. This is consistent with the results from a Spitzer study of CfA Seyferts (Deo et al. 2007), where sources with high $10\mu\text{m}$ silicate absorption show a preference for large host-galaxy inclinations and irregularities (merger events or interactions), both of which lead to absorption through the host.

In order to provide further clues on the extent of the MIR-absorbing material, we consider the [O III] 5007Å versus [O IV] line luminosity as shown in Figures 6 and 7. The features of the [O III] / [O IV] distribution are similar to those of $7\mu\text{m} / [\text{OIV}]$. Most Sy2s populate the same range as Sy1s, a few Sy2s show a [O III] deficit, i.e. on average about a factor 3 lower [O III] / [O IV] ratios when compared to Sy1s, consistent with results by Baum et al. (2010) on the $12\mu\text{m}$ sample. The distribution pattern of masers and non-masers appears to be statistically indistinguishable. A KS-test results in a probability of 61% that the Sy2 masers and non-masers are drawn from the same par-

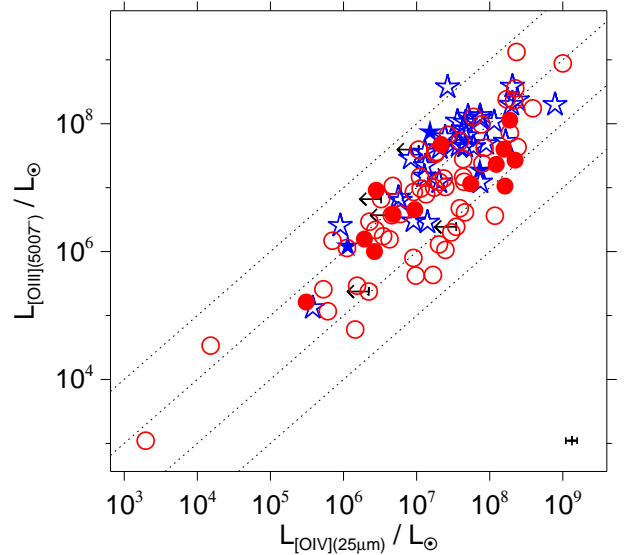


Fig. 6. Distribution of [O III] 5007Å versus [O IV] 25.9μm luminosity. Symbols are as in Figure 1. The dotted lines mark fixed-ratios 10; 1; 0.1; 0.01 (from top to bottom). The error-bar in the lower right corner is the average relative error of all [O IV] measurements.

ent population. However, the Sy2 subsample in Figures 6 and 7 shows a distinct tail towards lower ratios, potentially caused by absorption.

The [O IV] 25.9μm line is ~ 50 times less affected by extinction than the optical [O III] 5007Å line. A low [O III] / [O IV] ratio argues in favor of large obscuration, as explained in Haas et al. (2005). Another explanation of deviating [O III] / [O IV] ratios could be different radiation fields in the NLR. Because the [O IV] 25.9 μm line needs a higher ionization potential than the optical [O III] 5007Å line, AGN with a hard radiation field are expected to show a low ratio. The Sy2s

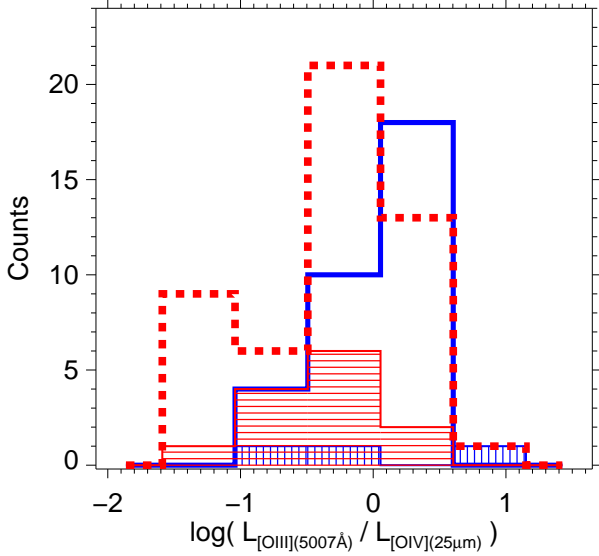


Fig. 7. Histogram of the [O III] to [O IV] ratio. Legend as in Fig. 2. Five upper limits are excluded.

with low [O III] / [O IV] would then be those AGN with hard radiation fields. But this is not consistent with other spectroscopic MIR tracers like the [Ne II] $12.8\mu\text{m}$ to [O IV] flux ratio (Meléndez et al. 2008b). Thus we conclude that in Figures 6 and 7 the NLR of Sy2s with [O III] deficit is considerably obscured.

While the [O III] obscuration may occur mainly in the innermost part of the NLR, the large extent (>1 kpc) of the NLR suggests that the absorption is not confined to the region encircled by the dust torus. Rather the sky-projected distribution of the absorbing material might reach further out to a considerable distance (several hundred parsec) from the line-of-sight to the nuclear accretion disk. The presence of moderately extended [O III] absorption, as well as the similarity of the $7\mu\text{m}$ / [O IV] and [O III] / [O IV] diagrams supports the picture that also the MIR absorption takes place in a moderately extended layer, i.e. the torus halo mentioned above. Although both observables $7\mu\text{m}$ and [O III] appear to be affected by absorption in a similar fashion, we note that the distribution of $7\mu\text{m}$ / [O III] spans a large range (2-700). This is not surprising in view of the diversity of the orientation-dependent appearance of the involved emitters and absorbers even for a simple AGN model.

3.3. Combined picture

Why do masers and non-masers show so different distributions in X-ray / [O IV], while their distribution in $7\mu\text{m}$ / [O IV] looks more similar?

Because masers need a large line-of-sight column density of velocity coherent gas, they are expected to be predominantly detected in edge-on accretion disks. Thus, the maser detection or non-detection can tell us about the disk orientation with respect to the line-of-sight. In order to constrain the implications in the framework of the AGN unified model, we consider two extreme cases:

1. For a disk seen edge-on, obviously the maser is most easily detected and the molecular torus is seen more or less edge-on, too. In this case the nuclear accretion disk (and its corona) is shielded by the torus, so that the X-rays are heavily obscured. If additional extended material, able to ob-

scure the MIR emission, does not lie in the torus plane, the $7\mu\text{m}$ / [O IV] ratio is decreased.

2. For a non-maser, both, disk and torus appear to be sufficiently tilted away from edge-on, so that the nuclear X-ray absorption is relatively low. In addition, our diagrams indicate the existence of non-masers, where the torus plane is seen edge-on, but the disk could be tilted out of this plane due to locally different angular momentum. In this case of a non-maser, the edge-on torus causes a high obscuration of the X-ray nucleus as well. On the other hand, irrespective of the disk and torus orientation, the MIR continuum can be absorbed or not depending on the line-of-sight through the extended host.

From these two extreme cases we see: While the requirement for heavy absorption of the nuclear X-rays is that the line-of-sight has to hit a rather compact area with very high column density, the area of the torus emission and even more the area of the (bright) NLR emission is orders of magnitude larger, so that the absorber must cover a larger area, too. If the absorption of X-rays and $7\mu\text{m}$ occurs on different spatial scales, the strength of the obscuration in each wavelength range may be sensitive to small differences in the aspect angle. Furthermore, because the MIR-absorbing material is located farther away from the line-of-sight to the nucleus, it is less reliable to predict whether a maser will be detected.

3.4. Comparison of the three samples with other known masers

Our combined sample was compiled from three complete samples with good coverage in the Spitzer archive. Table 1 shows the overlaps between the samples. Note that each sample is incomplete due to the limited availability of data in the Spitzer IRS archive and of X-Ray and [O III] measurements in the literature (see Tab. 2). Moreover, maser surveys were not performed with homogeneous properties (sensitivity, velocity coverage) and were not carried out for all sources of our combined sample.

The three samples were based on different selection criteria: Optically selected Seyferts in the CfA sample and IRAS selected sources in the $12\mu\text{m}$ and F25/F60 sample. Thus, it is possible that they suffer from different biases with respect to potential maser detection. The fraction of Sy2 masers to non-masers increases from 1/4 (4/16) in the CfA sample, to $\sim 1/3$ (11/29) in the $12\mu\text{m}$ sample and to ≥ 1 (8/6) in the IRAS F25/F60 sample. This is consistent with the well known fact that the mid- and far-infrared wavelengths select more obscured AGN than the optical bands.

However, the range of luminosity ratios ($L_X / L_{[\text{OIV}]}$, $L_{7\mu\text{m}} / L_{[\text{OIV}]}$, $L_{[\text{OIII}]} / L_{[\text{OIV}]}$), listed in Tab. 2, are similar for all three samples. This indicates that also among optical selected masing sources, some can be obscured with a level, similar to that of infrared selected sources⁵. To summarize, the result of all three samples (CfA, $12\mu\text{m}$ and IRAS F25/F60) are similar in that they point consistently to a prevalence of maser detections in Sy2s with high X-ray obscuration and one may expect this holds also for Seyfert galaxies in general.

Are our selected Sy2 masers representative for all 52 known Sy2 masers (Zhang et al. 2010)? To address this question, we compare our in-sample Sy2 masers with all remaining 37 off-sample Sy2 masers.

⁵ Even for infrared selected AGN, optical criteria influence the sample, because the Seyfert identification is done by optical spectroscopy.

In Figure 8 we show a comparison of X-ray and [OIV] luminosities between in- and off-sample masers. The comparison refers to those masers with X-ray and [OIV] fluxes available, i.e. 12 off-sample Sy2s 13 in-sample Sy2s and 3 in-sample Sy1s. Both, in-sample and off-sample roughly populate the same $L_X / L_{[OIV]}$ range. But the $L_X / L_{[OIV]}$ ratio is, on average, about a factor 2 higher for the off-sample than for the in-sample masers. This indicates that the off-sample Sy2 masers may be less absorbed than the in-sample ones. Compared with the in-sample Sy2 non-masers (omitted in Fig 8, see Fig. 1), however, the off-sample masers show, on average, still about a factor 2 lower $L_X / L_{[OIV]}$, hence considerably high obscuration.

Some off-sample masers show spurious flux ratios that imply no obscuration (i.e. $L_X / L_{[OIV]} > 10$ for 4 objects). Among them, we find two nearby extended sources, NGC4258 and NGC4945, in which the X-ray emission has been associated with star formation by Risaliti (2002) and Strickland et al. (2004).

To summarize, the large overlap and the lack of significant differences between in- and off-sample Sy2 masers indicates that the results for our combined sample's Sy2 masers can be extended to all known Sy2 masers.

We note that the inhomogeneous selection of all off-sample masers and non-masers precludes to derive a meaningful comparison of maser to non-maser statistics with our in-sample data. A KS test shows a probability of 63% that both subsets, off- and in-sample masers, are drawn from the same parent distribution and the above mentioned difference in $L_X / L_{[OIV]}$ is only by chance. But similarly a KS test between the in-sample non-masers and the off-sample masers yields also 60% probability that they are drawn from the same parent distribution. But yet, comparing the $L_X / L_{[OIV]}$ ratio between in-sample Sy1 non-masers and the off-sample Sy2 masers, shows a probability of 0.16% to be drawn from the same parent distribution. This shows that the off-sample Sy2 masers are still significantly different from the unobscured Sy1 non-maser.

3.5. Maser and AGN luminosity

A search for H₂O masers in 274 high-redshift ($0.3 < z < 0.8$) SDSS type-2 AGN half of which being type-2 *quasars* (Bennert et al. 2009) found only one maser (SDSSJ0804+3607, Barvainis & Antonucci 2005). The high rate of non-detections in these luminous AGN could be due to limited observational sensitivity or to intrinsic differences between low- and high-luminosity AGN. Such differences could be, for instance, that in a high-luminosity AGN the accretion disk becomes hotter so that the density required for maser emission falls below a critical limit. If this is frequently the case, one would expect a relative decline of H₂O maser luminosity with increasing AGN luminosity. On the other hand, the SDSS H₂O maser survey was relatively shallow, because one was interested to find masers which are sufficiently bright for spatially resolved follow-up VLBI observations.

Here, we consider how far the Seyfert sample can help to distinguish between these two possibilities (i.e. by looking whether or not $L_{H_2O} / L_{[OIV]}$ declines with increasing $L_{[OIV]}$). A remarkable feature of Fig. 1 is that maser-detections and non-detections are quite evenly distributed along the whole [OIV] luminosity range covering about 4 orders of magnitude. Thus our data do not indicate a trend that the frequency of non-masers rises with luminosity. We have also seen that the available maser observations of the Seyferts are biased against maser detection in faint (and distant) AGN (Fig. 4).

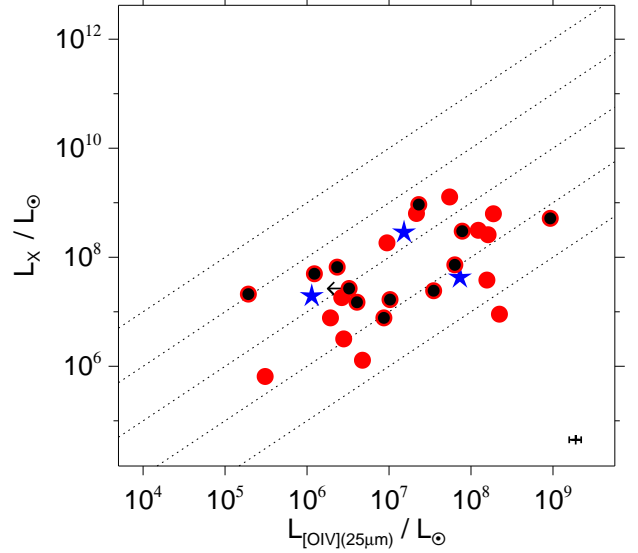


Fig. 8. Observed 2-10 keV X-rays plotted against [OIV] line luminosity. Sy1 masers are represented by blue stars and Sy2 masers by red dots. Off-sample Sy2 masers are marked with black dots. The dotted lines mark fixed flux ratios of 1000; 100; 10; 1; 0.1 (from top to bottom). The error-bar in the lower right corner is the average relative error of all [OIV] measurements.

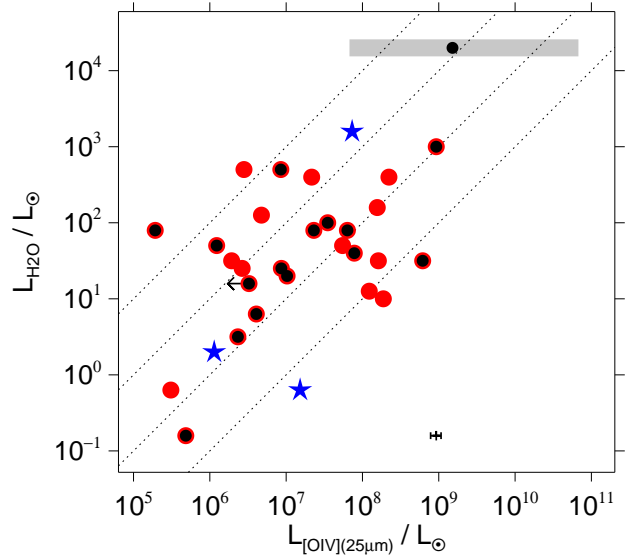


Fig. 9. Maser H₂O versus [OIV] luminosity. Symbols and colors are as in Fig. 8. The dotted lines mark fixed-ratios 10^{-4} ; 10^{-5} ; 10^{-6} ; 10^{-7} (from top to bottom). For comparison, the expected position of the $z = 0.66$ maser SDSSJ0804+3607 is marked with a black dot and a gray bar covering the range $0.1 \times L_{[OIII]} < L_{[OIV]} < 100 \times L_{[OIII]}$ assumed from Fig. 6.

Figure 9 shows the (isotropic) maser luminosity versus the AGN luminosity as traced by [OIV]. In addition to the Seyfert sample we have plotted the expected position of SDSSJ0804+3607 at $z = 0.66$, the only QSO-2 maser detection. Because this source was not observed with Spitzer IRS, we derived $L_{[OIV]}$ from $L_{[OIII]}$ using the range $0.1 \times L_{[OIII]} < L_{[OIV]} < 100 \times L_{[OIII]}$ as indicated in Fig. 6, which is also

valid for higher-luminosity AGN (Haas et al. 2005). At a given [OIV] luminosity the maser luminosity spreads over three orders of magnitude (Fig. 9). One explanation for the large spread is that the maser emission is, in fact, not isotropic and hence the derived maser luminosity depends sensitively on the maser direction with respect to the line-of-sight. The Seyfert sample alone indicates only a marginal correlation in Fig. 9, with a Pearson correlation coefficient of 0.32 for all Sy2 masers of our combined sample that is not significant at the 5% level. Adding the off-sample Sy2 masers changes the coefficient to 0.46 which would then be significant, but the correlation could also be an artifact of distance in the luminosities. However, combined with the position of SDSSJ0804+3607 and the fact, that its assumed H_2O / [OIV] ratio lies in the same range as for the lower luminosity AGN, argues in favor of a physical connection between maser and AGN luminosity.

The numerous non-masers among the SDSS QSO-2s (Bennert et al. 2009) have a [OIII] luminosity similar to that of SDSSJ0804+3607, hence are expected to populate a similar $L_{[OIV]}$ range in Fig. 9. The H_2O maser upper limits⁶, found for these QSO-2s by Bennert et al. (2009), lie even above J0804+3607.

Thus the upper limits are not stringent enough to support a relative decline of maser luminosity with increasing AGN luminosity. This, together with the sufficiently high $L_{H_2O} / L_{[OIV]}$ ratio of J0804+3607, leads us to conclude that the main reason for the high rate of maser non-detections is insufficient observational sensitivity, rather than basic differences between low- and high-luminosity AGN for hosting a maser.

4. Conclusion

In order to understand the connection between H_2O maser detection rate and nuclear extinction we used the [OIV]_{25.9 μm} line and the 7 μm continuum flux from Spitzer spectra of a well-selected sample of 114 Seyfert galaxies, from the CfA, 12 μm and IRAS F25/F60 catalogs, for which a maser search has been performed. These data were then compared to hard X-ray and [OIII] 5007 Å fluxes from the literature. We analyzed the data in the framework of the orientation-dependent AGN unified scheme, yielding the following results:

1. Comparing hard X-rays to [OIV] flux, Sy2s exhibit, on average, an about 10 times lower X-ray to [OIV] ratio than Sy1s. Masers prefer X-ray absorbed sources (i. e. low $L_X / L_{[OIV]}$ ratios). Sy2 masers present on average about 4 times less X-ray flux normalized by [OIV] than non-maser Sy2s. This is consistent with geometric alignment of both the X-ray absorber and the maser emitting region in the accretion disk. Non-masers do not show a preference for strongly absorbed sources. However, our data indicate an observational bias against faint sources, in the sense that more sensitive maser observations might reveal more absorbed sources to house a maser.
2. Regarding the 7 μm to [OIV] flux ratio we find that most Sy2s spread along the same range as Sy1s. However there are sources with a significantly lower ratio, rendering the Sy2s on average about 3 times lower than Sy1s. These cases can be explained by an extended dusty absorber that is covering the 7 μm emitting torus region. Maser-detections also show a preference for 7 μm absorbed sources, but with less significance than in the X-ray to [OIV] comparison. This suggests

that the geometric alignment of the MIR absorber with the maser emitting disk is not as perfect as the supposed alignment of the disk with the X-ray absorber.

3. The [OIII] to [OIV] flux ratio also indicates the presence of extended obscuration in some Sy2s that blocks the optical emission from the NLR. Masers and non-masers are distributed very similarly in the [OIII] to [OIV] plot. The fraction of maser-detections is not significantly higher for sources with such extended absorption. This leads us to conclude that the matter distribution for the [OIII] absorber is not essential for the prediction of a maser detection. Moreover, it is possible that a substantial fraction of the absorption of AGN emission could occur in extended regions outside the torus that are not necessarily aligned with the torus or AGN sub-structure.
4. The three samples, CfA, 12 μm and IRAS F25/F60 provide very similar results. The Sy2 maser to non-maser fraction increases from optical to infrared selection. The Sy2 masers of our combined sample have a similar range of $L_{[OIV]}$ and L_{H_2O} as the known off-sample Sy2 masers. While, on average, the off-sample masers are a factor two less obscured, as inferred by the $L_X / L_{[OIV]}$ ratio, they are still considerably obscured compared with Sy1s from our combined sample. Thus, the results obtained for our combined sample's Sy2 masers may also hold for all remaining Sy2 maser sources that have no Spitzer or X-ray data available.
5. After supplementing our combined sample with the remaining known Sy2 masers that were not included in it, the H_2O maser luminosity appears to be correlated with the AGN luminosity as traced by [OIV], although with a large spread. We do not find evidence for physical differences between low- and high-luminosity AGN for housing a maser.

The results demonstrate that heavy X-ray absorption is an indicator for high probability to detect a maser. The 7 μm absorption can also be used to find maser candidates, but with lower probability.

Acknowledgements. The work is based on observations made with the *Spitzer Space Telescope*, which is operated by the Jet Propulsion Laboratory, California Institute of Technology under a contract with NASA. This research has made use of the NASA/IPAC Extragalactic Database (NED) which is operated by the Jet Propulsion Laboratory, California Institute of Technology, under contract with the National Aeronautics and Space Administration. This publication is supported as a project of the Nordrhein-Westfälische Akademie der Wissenschaften und der Künste in the framework of the academy program by the Federal Republic of Germany and the state Nordrhein-Westfalen. We thank the referee J. S. Zhang for his careful review of the manuscript.

References

- Alonso-Herrero, A., Ward, M. J., & Kotilainen, J. K. 1997, MNRAS, 288, 977
 Antonucci, R. 1993, ARA&A, 31, 473
 Awaki, H., Ueno, S., Taniguchi, Y., & Weaver, K. A. 2000, ApJ, 542, 175
 Baker, J. C. 1997, MNRAS, 286, 23
 Barvainis, R. & Antonucci, R. 2005, ApJ, 628, L89
 Bassani, L., Dadina, M., Maiolino, R., et al. 1999, ApJS, 121, 473
 Baum, S. A., Gallimore, J. F., O'Dea, C. P., et al. 2010, ApJ, 710, 289
 Becker, R., Henkel, C., Wilson, T. L., & Wouterloot, J. G. A. 1993, A&A, 268, 483
 Bennert, N., Barvainis, R., Henkel, C., & Antonucci, R. 2009, ApJ, 695, 276
 Bennert, N., Falcke, H., Schulz, H., Wilson, A. S., & Wills, B. J. 2002, ApJ, 574, L105
 Bennert, N., Jungwiert, B., Komossa, S., Haas, M., & Chini, R. 2006, A&A, 446, 919
 Bianchi, S., Balestra, I., Matt, G., Guainazzi, M., & Perola, G. C. 2003, A&A, 402, 141
 Bianchi, S., Miniutti, G., Fabian, A. C., & Iwasawa, K. 2005, MNRAS, 360, 380
 Blustin, A. J., Branduardi-Raymont, G., Behar, E., et al. 2002, A&A, 392, 453

⁶ $\frac{L_{H_2O}}{L_{\odot}} = 0.0039 \times \frac{1}{1+z} \times \left(\frac{D_L}{\text{Mpc}}\right)^2$

- Boroson, T. A. & Meyers, K. A. 1992, *ApJ*, 397, 442
- Braatz, J. 2008, in *A Decade of Dark Energy*
- Braatz, J. A. & Gugliucci, N. E. 2008, *ApJ*, 678, 96
- Braatz, J. A., Henkel, C., Greenhill, L. J., Moran, J. M., & Wilson, A. S. 2004, *ApJ*, 617, L29
- Braatz, J. A., Wilson, A. S., & Henkel, C. 1996, *ApJS*, 106, 51
- Braatz, J. A., Wilson, A. S., & Henkel, C. 1997, *ApJS*, 110, 321
- Braatz, J. A., Wilson, A. S., Henkel, C., Gough, R., & Sinclair, M. 2003, *ApJS*, 146, 249
- Braito, V., Franceschini, A., Della Ceca, R., et al. 2003, *A&A*, 398, 107
- Buchanan, C. L., Gallimore, J. F., O'Dea, C. P., et al. 2006, *AJ*, 132, 401
- Cappi, M., Panessa, F., Bassani, L., et al. 2006, *A&A*, 446, 459
- Claussen, M. J. & Lo, K. 1986, *ApJ*, 308, 592
- Dahari, O. & De Robertis, M. M. 1988, *ApJS*, 67, 249
- de Grijs, M. H. K., Keel, W. C., Miley, G. K., Goudfrooij, P., & Lub, J. 1992, *A&AS*, 96, 389
- Deo, R. P., Crenshaw, D. M., Kraemer, S. B., et al. 2007, *ApJ*, 671, 124
- Deo, R. P., Richards, G. T., Crenshaw, D. M., & Kraemer, S. B. 2009, *ApJ*, 705, 14
- di Serego Alighieri, S., Cimatti, A., Fosbury, R. A. E., & Hes, R. 1997, *A&A*, 328, 510
- Done, C., Madejski, G. M., Życki, P. T., & Greenhill, L. J. 2003, *ApJ*, 588, 763
- Elitzur, M. 2002, in *IAU Symposium*, Vol. 206, *Cosmic Masers: From Proto-Stars to Black Holes*, ed. V. Migenes & M. J. Reid, 452–+
- Genzel, R., Lutz, D., Sturm, E., et al. 1998, *ApJ*, 498, 579
- Gondoin, P., Barr, P., Lumb, D., et al. 2001, *A&A*, 378, 806
- Gondoin, P., Orr, A., & Lumb, D. 2003a, *A&A*, 398, 967
- Gondoin, P., Orr, A., Lumb, D., & Santos-Lleo, M. 2002, *A&A*, 388, 74
- Gondoin, P., Orr, A., Lumb, D., & Siddiqui, H. 2003b, *A&A*, 397, 883
- González-Martín, O., Masegosa, J., Márquez, I., Guerrero, M. A., & Dultzin-Hacyan, D. 2006, *A&A*, 460, 45
- Greenhill, L. J., Ellingsen, S. P., Norris, R. P., et al. 2002, *ApJ*, 565, 836
- Greenhill, L. J., Henkel, C., Becker, R., Wilson, T. L., & Wouterloot, J. G. A. 1995, *A&A*, 304, 21
- Greenhill, L. J., Herrnstein, J. R., Moran, J. M., Menten, K. M., & Velusamy, T. 1997, *ApJ*, 486, L15+
- Greenhill, L. J., Moran, J. M., Reid, M. J., et al. 1990, *ApJ*, 364, 513
- Greenhill, L. J., Moran, J. M., Reid, M. J., Menten, K. M., & Hirabayashi, H. 1993, *ApJ*, 406, 482
- Greenhill, L. J., Tilak, A., & Madejski, G. 2008, *ApJ*, 686, L13
- Gu, Q., Melnick, J., Fernandes, R. C., et al. 2006, *VizieR Online Data Catalog*, 736, 60480
- Guainazzi, M., Matt, G., & Perola, G. C. 2005, *A&A*, 444, 119
- Haas, M., Siebenmorgen, R., Schulz, B., Krügel, E., & Chini, R. 2005, *A&A*, 442, L39
- Hagiwara, Y., Diamond, P. J., & Miyoshi, M. 2002, *A&A*, 383, 65
- Hagiwara, Y., Diamond, P. J., Miyoshi, M., Rovilos, E., & Baan, W. 2003, *MNRAS*, 344, L53
- Haschick, A. D. & Baan, W. A. 1985, *Nature*, 314, 144
- Heckman, T. M., Crane, P. C., & Balick, B. 1980, *A&AS*, 40, 295
- Heckman, T. M., Ptak, A., Hornschemeier, A., & Kauffmann, G. 2005, *ApJ*, 634, 161
- Henkel, C. 2008, in *A Decade of Dark Energy*
- Henkel, C., Guesten, R., Downes, D., et al. 1984, *A&A*, 141, L1
- Henkel, C., Peck, A. B., Tarchi, A., et al. 2005, *A&A*, 436, 75
- Henkel, C., Wang, Y. P., Falcke, H., Wilson, A. S., & Braatz, J. A. 1998, *A&A*, 335, 463
- Henkel, C., Wouterloot, J. G. A., & Bally, J. 1986, *A&A*, 155, 193
- Herrnstein, J. R., Moran, J. M., Greenhill, L. J., et al. 1999, *Nature*, 400, 539
- Hes, R., Barthel, P. D., & Fosbury, R. A. E. 1996, *A&A*, 313, 423
- Ho, L. C. 2005, *ApJ*, 629, 680
- Ho, L. C., Filippenko, A. V., & Sargent, W. L. 1995, *ApJS*, 98, 477
- Ho, L. C., Filippenko, A. V., & Sargent, W. L. W. 1997, *ApJS*, 112, 315
- Holczer, T., Behar, E., & Kaspi, S. 2007, *ApJ*, 663, 799
- Huchra, J. & Burg, R. 1992, *apj*, 393, 90
- Immler, S., Brandt, W. N., Vignali, C., et al. 2003, *AJ*, 126, 153
- Iyomoto, N., Makishima, K., Fukazawa, Y., et al. 1996, *PASJ*, 48, 231
- Kewley, L. J., Heisler, C. A., Dopita, M. A., & Lumsden, S. 2001, *ApJS*, 132, 37
- Kim, D., Sanders, D. B., Veilleux, S., Mazzarella, J. M., & Soifer, B. T. 1995, *ApJS*, 98, 129
- Kondratko, P. T., Greenhill, L. J., & Moran, J. M. 2006a, *ApJ*, 652, 136
- Kondratko, P. T., Greenhill, L. J., Moran, J. M., et al. 2006b, *ApJ*, 649, 561
- Lamastra, A., Bianchi, S., Matt, G., et al. 2009, *A&A*, 504, 73
- Lawson, A. J. & Turner, M. J. L. 1997, *MNRAS*, 288, 920
- Levenson, N. A., Heckman, T. M., Krolik, J. H., Weaver, K. A., & Życki, P. T. 2006, *ApJ*, 648, 111
- Lo, K. Y. 2005, *ARA&A*, 43, 625
- Lumsden, S. L. & Alexander, D. M. 2001, *MNRAS*, 328, L32
- Lumsden, S. L., Alexander, D. M., & Hough, J. H. 2004, *MNRAS*, 348, 1451
- Maiolino, R. & Rieke, G. H. 1995, *ApJ*, 454, 95
- Malizia, A., Landi, R., Bassani, L., et al. 2007, *ApJ*, 668, 81
- Matsumoto, C., Nava, A., Maddox, L. A., et al. 2004, *ApJ*, 617, 930
- Matt, G., Perola, G. C., Fiore, F., et al. 2000, *A&A*, 363, 863
- Meléndez, M., Kraemer, S. B., Armentrout, B. K., et al. 2008a, *ApJ*, 682, 94
- Meléndez, M., Kraemer, S. B., Schmitt, H. R., et al. 2008b, *ApJ*, 689, 95
- Miniutti, G., Ponti, G., Dadina, M., Cappi, M., & Malaguti, G. 2007, *MNRAS*, 375, 227
- Moustakas, J. & Kennicutt, Jr., R. C. 2006, *ApJS*, 164, 81
- Mulchaey, J. S., Koratkar, A., Ward, M. J., et al. 1994, *ApJ*, 436, 586
- Nakai, N., Inoue, M., Miyazawa, K., Miyoshi, M., & Hall, P. 1995, *PASJ*, 47, 771
- Nandra, K., O'Neill, P. M., George, I. M., & Reeves, J. N. 2007, *MNRAS*, 382, 194
- Nenkova, M., Sirocky, M. M., Ivezić, Ž., & Elitzur, M. 2008, *ApJ*, 685, 147
- Netzer, H., Mainieri, V., Rosati, P., & Trakhtenbrot, B. 2006, *A&A*, 453, 525
- Oliva, E., Salvati, M., Moorwood, A. F. M., & Marconi, A. 1994, *A&A*, 288, 457
- Panessa, F., Bassani, L., Cappi, M., et al. 2006, *A&A*, 455, 173
- Perola, G. C., Matt, G., Cappi, M., et al. 2002, *A&A*, 389, 802
- Perola, G. C., Matt, G., Fiore, F., et al. 2000, *A&A*, 358, 117
- Phillips, M. M., Charles, P. A., & Baldwin, J. A. 1983, *ApJ*, 266, 485
- Polletta, M., Bassani, L., Malaguti, G., Palumbo, G. G. C., & Caroli, E. 1996, *ApJS*, 106, 399
- Ramolla, M. 2009, *Middle-Infrared Spectroscopy of Seyfert Galaxies*, Diploma Thesis, Ruhr-Universität Bochum
- Rao, A. R., Singh, K. P., & Vahia, M. N. 1992, *MNRAS*, 255, 197
- Reeves, J. N. & Turner, M. J. L. 2000, *MNRAS*, 316, 234
- Reynolds, C. S. 1997, *MNRAS*, 286, 513
- Risaliti, G. 2002, *A&A*, 386, 379
- Risaliti, G., Gilli, R., Maiolino, R., & Salvati, M. 2000, *A&A*, 357, 13
- Rush, B. & Malkan, M. A. 1993, in *Bulletin of the American Astronomical Society*, Vol. 25, *Bulletin of the American Astronomical Society*, 1362–+
- Sato, N., Yamauchi, A., Ishihara, Y., et al. 2005, *PASJ*, 57, 587
- Schmitt, H. R., Donley, J. L., Antonucci, R. R. J., Hutchings, J. B., & Kinney, A. L. 2003, *ApJS*, 148, 327
- Schweitzer, M., Lutz, D., Sturm, E., et al. 2006, *ApJ*, 649, 79
- Severgnini, P., Risaliti, G., Marconi, A., Maiolino, R., & Salvati, M. 2001, *A&A*, 368, 44
- Shang, Z., Wills, B. J., Wills, D., & Brotherton, M. S. 2007, *AJ*, 134, 294
- Sharples, R. M., Longmore, A. J., Hawarden, T. G., & Carter, D. 1984, *MNRAS*, 208, 15
- Shinozaki, K., Miyaji, T., Ishisaki, Y., Ueda, Y., & Ogasaka, Y. 2006, *AJ*, 131, 2843
- Shu, X. W., Wang, J. X., Jiang, P., Fan, L. L., & Wang, T. G. 2007, *ApJ*, 657, 167
- Smith, D. A. & Wilson, A. S. 2001, *ApJ*, 557, 180
- Smith, J. D. T. & Draine, B. T. 2008, *PAHFIT web description*, <http://tir.astro.utoledo.edu/jdsmith/research/pahfit.php>
- Smith, J. D. T., Draine, B. T., Dale, D. A., et al. 2007, *ApJ*, 656, 770
- Spinoglio, L. & Malkan, M. A. 1989, *ApJ*, 342, 83
- Storchi-Bergmann, T., Kinney, A. L., & Challis, P. 1995, *ApJS*, 98, 103
- Strickland, D. K., Heckman, T. M., Colbert, E. J. M., Hoopes, C. G., & Weaver, K. A. 2004, *ApJS*, 151, 193
- Terashima, Y., Iyomoto, N., Ho, L. C., & Ptak, A. F. 2002, *ApJS*, 139, 1
- Tilak, A., Greenhill, L. J., Done, C., & Madejski, G. 2008, *ApJ*, 678, 701
- Tommasin, S., Spinoglio, L., Malkan, M. A., & Fazio, G. 2010, *ApJ*, 709, 1257
- Tran, H. D. 2003a, *ApJ*, 583, 632
- Tran, H. T. 2003b, *New Astronomy Review*, 47, 1091
- Turner, T. J., George, I. M., Nandra, K., & Mushotzky, R. F. 1997, *ApJS*, 113, 23
- Turner, T. J. & Pounds, K. A. 1989, *MNRAS*, 240, 833
- Ueda, Y., Ishisaki, Y., Takahashi, T., Makishima, K., & Ohashi, T. 2005, *ApJS*, 161, 185
- Ueno, S., Ward, M. J., O'Brien, P. T., Stirpe, G. M., & Matt, G. 2000, *Advances in Space Research*, 25, 823
- Vaceli, M. S., Viegas, S. M., Gruenwald, R., & de Souza, R. E. 1997, *AJ*, 114, 1345
- Véron-Cetty, M. & Véron, P. 2006, *A&A*, 455, 773
- Verrecchia, F., in't Zand, J. J. M., Giommi, P., et al. 2007, *A&A*, 472, 705
- Whittle, M. 1992, *ApJS*, 79, 49
- Whittle, M. & Wilson, A. S. 2004, *AJ*, 127, 606
- Zhang, J. S. & Fan, J. H. 2009, *Sci Chin.*, 52, G6, 960
- Zhang, J. S., Henkel, C., Guo, Q., Wang, H. G., & Fan, J. H. 2010, *ApJ*, 708, 1528
- Zhang, J. S., Henkel, C., Kadler, M., et al. 2006, *A&A*, 450, 933

(1)	(2)	(3)	(4)	(5)	(6)	(7)
Intersecting sample	CfA	12 μ m	IRAS	12 μ m \cup IRAS	CfA \cup IRAS	CfA \cup 12 μ m
CfA	54	42	12	45	–	–
12 μ m	–	118	24	–	57	–
IRAS F25/F60	–	–	60	–	–	27

Table 1. Documentation of how far the three samples (of 163 sources in total) match and complement each other. For each row the Table entries list the number of sources contained in the intersection of the sample denoted by the columns 2-7 with the CfA, 12 μ m and IRAS F25/F60 sample (Col. 1). E. g. the union of the 12 μ m and IRAS F25/F60 samples (Col. 5) has 45 sources in common with the CfA sample (Row 1).

(1)		(2)		(3)		(4)		(5)
		$L_X / L_{[OIV]}$		$L_{7\mu m} / L_{[OIV]}$		$L_{[OIII]} / L_{[OIV]}$		Parent Sample
Parent Sample	Subset	Number	log(Ratio)	Number	log(Ratio)	Number	log(Ratio)	Number
CfA	Sy1 maser	3	0.8 ± 0.9	3	1.6 ± 0.1	3	0.0 ± 0.6	3
	Sy1 non-maser	16	2.0 ± 0.5	14	1.9 ± 0.5	16	0.1 ± 0.4	18
	Sy1 unknown	2	1.73 ± 0.02	3	2.1 ± 0.6	2	-0.1 ± 0.1	4
	Sy2 maser	4	0.1 ± 0.5	4	1.2 ± 0.7	4	-0.2 ± 0.6	4
	Sy2 non-maser	16	1.1 ± 0.9	18	1.3 ± 0.5	20	-0.2 ± 0.5	24
	Sy2 unknown	0	–	1	1.4	1	–1.3	1
12 μ m	Sy1 maser	2	1.25 ± 0.93	2	1.6 ± 0.1	2	0.4 ± 0.5	2
	Sy1 non-maser	22	2.0 ± 0.6	22	1.8 ± 0.5	27	0.1 ± 0.4	30
	Sy1 unknown	4	2.3 ± 0.6	5	1.9 ± 0.6	6	0.0 ± 0.3	9
	Sy2 maser	11	0.5 ± 0.7	10	1.2 ± 0.6	11	-0.3 ± 0.5	13
	Sy2 non-maser	29	0.9 ± 1.0	34	1.4 ± 0.5	42	-0.4 ± 0.6	51
	Sy2 unknown	1	1.1	1	1.4	2	-0.7 ± 0.9	2
IRAS	Sy1 maser	0	–	0	–	0	–	0
	Sy1 non-maser	13	2.2 ± 0.4	10	1.7 ± 0.3	15	0.0 ± 0.4	15
	Sy1 unknown	0	–	0	–	0	–	0
	Sy2 maser	8	0.2 ± 1.0	8	1.2 ± 0.7	8	-0.3 ± 0.4	8
	Sy2 non-maser	6	0.7 ± 0.8	9	1.3 ± 0.5	10	-0.2 ± 0.5	11
	Sy2 unknown	0	–	0	–	0	–	0
Combined: CfA \cup 12 μ m \cup IRAS	Sy1 maser	3	$.8 \pm 0.9$	3	1.6 ± 0.1	3	0.0 ± 0.6	3
	Sy1 non-maser	28	2.0 ± 0.6	25	1.8 ± 0.5	33	0.1 ± 0.4	36
	Sy1 unknown	5	2.1 ± 0.6	6	1.9 ± 0.5	7	0.0 ± 0.3	10
	Sy2 maser	13	0.4 ± 0.8	12	1.1 ± 0.6	13	-0.4 ± 0.5	15
	Sy2 non-maser	32	0.9 ± 1.0	42	1.4 ± 0.5	50	-0.3 ± 0.6	60
	Sy2 unknown	1	1.1	1	1.4	2	-0.7 ± 0.9	2

Table 2. The average values and standard deviations of the logarithmic luminosity ratios for each subset of Seyfert galaxies. Column 1: In descending order, the optically selected CfA sources (Huchra & Burg 1992), the MIR selected 12 μ m sources (Rush & Malkan 1993), the IRAS F25/F60 flux-ratio selected sources (Schmitt et al. 2003) and the combined sample that is used in this work. Columns 2-4: Number of sources with luminosities available in [OIV] and one of the following: 2-10 keV X-rays (Col. 2) or 7 μ m (Col. 3) or [OIII] (Col. 4). Each sample's row is subdivided into Sy1 maser, non-maser, maser-unknown and Sy2 maser, non-maser, maser-unknown. Column 5: Total Number of objects of the parent sample from Col. 1, e.g. 3 Sy1 maser in the CfA, 18 Sy1 non-maser in the CfA and so forth.

(1)	(2)	(3)	(4)	(5)	(6)	(7)	Source	H ₂ O	Sy	[O IV]	[O III]	2-10 keV	7.6 μ m
Source	H ₂ O	Sy	[O IV]	[O III]	2-10 keV	7.6 μ m							
	$\log\left(\frac{L}{L_{\odot}}\right)$		$(10^{-15} \frac{\text{erg}}{\text{s cm}^2})$	$(10^{-14} \frac{\text{erg}}{\text{s cm}^2})$									
MRK334 ^[a]	–	1.8	82 ± 14	49 ^[1]	800 ^[2]	504 ± 101	NGC4569 ^[a]	–	2.0	42 ± 10	24 ^[5]	–	463 ± 95
MRK335 ^[a,b]	–	1.0	67 ± 10	950 ^[3]	960 ^[4]	983 ± 241	NGC4579 ^[a,b]	–	1.9	30 ± 5	–	440 ^[29]	325 ± 74
MRK938 ^[b]	*	2.0	–	44 ^[5]	23 ^[6]	332 ± 66	NGC4593 ^[b,c]	–	1.0	127 ± 40	134 ^[8]	3710 ^[42]	1428 ± 304
E12-G21 ^[b]	?	1.0	187 ± 56	97 ^[7]	–	366 ± 82	NGC4602 ^[b]	–	1.9	< 66	134 ^[8]	–	70 ± 18
MRK348 ^[b,c]	2.6	2.0	163 ± 25	359 ^[8]	482 ^[9]	1151 ± 235	TOL1238-364 ^[b]	–	2.0	145 ± 23	194 ^[18]	17 ^[11]	779 ± 161
IZw1 ^[b]	?	1.0	97 ± 13	44 ^[1]	680 ^[10]	–	M-2-33-34 ^[b]	–	1.0	670 ± 145	364 ^[8]	–	175 ± 57
IRAS00521-7054 ^[b]	–	2.0	71 ± 11	77 ^[8]	–	–	MRK231 ^[b]	–	1.0	233 ± 70	230 ^[1]	68 ^[11]	5960 ± 1192
NGC424 ^[b]	–	2.0	223 ± 34	420 ^[3]	122 ^[11]	3655 ± 738	NGC4826 ^[a]	–	2.0	139 ± 41	–	–	540 ± 108
NGC526A ^[b]	–	1.5	176 ± 26	270 ^[3]	2046 ^[11]	669 ± 162	NGC4922 ^[b]	2.3	2.0	–	64 ^[5]	–	476 ± 96
NGC513 ^[b]	–	2.0	59 ± 9	35 ^[12]	–	232 ± 59	NGC4941 ^[b]	–	2.0	285 ± 43	143 ^[18]	82 ^[11]	< 513
F01475-0740 ^[b,c]	–	2.0	62 ± 10	53 ^[8]	82 ^[13]	393 ± 111	NGC4968 ^[b,c]	–	2.0	307 ± 45	177 ^[8]	15 ^[13]	742 ± 156
UM146 ^[a]	–	1.9	26 ± 3	60 ^[3]	–	< 199	NGC5005 ^[a,b]	–	2.0	179 ± 21	7 ^[1]	–	344 ± 69
MRK590 ^[c]	–	1.2	31 ± 8	53 ^[1]	1970 ^[14]	< 589	NGC5033 ^[a,b]	–	1.8	109 ± 23	53 ^[1]	550 ^[29]	211 ± 43
MCG+05-06-036 ^[a,b]	?	1.0	42 ± 5	–	–	166 ± 33	MCG-03-34-064 ^[a,b]	–	1.8	1062 ± 153	1507 ^[8]	210 ^[43]	2206 ± 442
NGC931 ^[b,c]	–	1.5	459 ± 67	75 ^[8]	2000 ^[15]	1697 ± 392	NGC5135 ^[b]	–	2.0	726 ± 147	219 ^[44]	–	808 ± 161
NGC1068 ^[a,b,c]	2.2	2.0	18908 ± 2697	4834 ^[8]	462 ^[16]	52585 ± 10567	NGC5194 ^[b]	–0.2	2.0	227 ± 47	120 ^[34]	48 ^[16]	199 ± 46
NGC1056 ^[b]	–	2.0	< 212	23 ^[7]	–	235 ± 47	M-6-30-15 ^[b,c]	–	1.2	227 ± 34	75 ^[19]	4220 ^[37]	1425 ± 313
NGC1097 ^[a,b]	–	1.0	52 ± 12	18 ^[7]	170 ^[17]	283 ± 58	IRAS13349+2438 ^[a,b]	?	1.0	64 ± 9	47 ^[7]	360 ^[45]	3194 ± 673
NGC1125 ^[b]	–	2.0	356 ± 52	23 ^[18]	–	118 ± 27	MRK266 ^[b]	1.5	2.0	349 ± 77	23 ^[34]	56 ^[23]	72 ± 14
NGC1144 ^[b]	–	2.0	69 ± 10	–	11000 ^[2]	164 ± 37	MRK273 ^[a,b]	–	2.0	474 ± 142	213 ^[5]	60 ^[29]	–
M-2-8-39 ^[b,c]	–	2.0	144 ± 21	183 ^[8]	–	270 ± 69	IC4329a ^[a,b]	–	1.2	1061 ± 156	340 ^[12]	16400 ^[46]	4140 ± 968
NGC1194 ^[b,c]	–	1.0	144 ± 21	396 ^[19]	–	521 ± 105	NGC5347 ^[a,b,c]	1.5	2.0	54 ± 9	45 ^[8]	22 ^[47]	628 ± 129
NGC1241 ^[b]	–	2.0	< 100	370 ^[20]	–	–	MRK463E ^[a,b]	–	2.0	639 ± 96	563 ^[1]	40 ^[29]	2295 ± 461
NGC1320 ^[b,c]	*	2.0	254 ± 37	122 ^[8]	496 ^[21]	933 ± 231	NGC5506 ^[b]	1.7	1.9	2492 ± 360	521 ^[28]	5800 ^[48]	4222 ± 844
NGC1365 ^[b]	–	1.8	1441 ± 207	62 ^[22]	660 ^[23]	2759 ± 553	NGC5548 ^[a,b,c]	–	1.5	141 ± 24	360 ^[8]	4300 ^[49]	726 ± 174
NGC1386 ^[b,c]	2.1	2.0	991 ± 145	800 ^[24]	27 ^[18]	1017 ± 206	MRK817 ^[a,b]	–	1.5	73 ± 12	140 ^[1]	–	950 ± 244
IRAS03362-1641 ^[b]	–	2.0	52 ± 8	18 ^[8]	–	–	PG1501+106 ^[a]	–	1.5	246 ± 36	250 ^[1]	1869 ^[11]	–
F03450+0055 ^[b]	?	1.5	31 ± 5	100 ^[25]	–	< 10504	NGC5929 ^[a,b]	–	2.0	< 114	93 ^[1]	197 ^[11]	32 ± 8
3C120 ^[a,b]	–	1.0	1195 ± 174	304 ^[8]	8200 ^[26]	987 ± 235	NGC5953 ^[b]	–	2.0	172 ± 25	63 ^[3]	–	259 ± 52
MRK618 ^[b]	–	1.0	96 ± 16	160 ^[8]	700 ^[27]	–	M-2-40-4 ^[b]	–	2.0	115 ± 19	74 ^[12]	2693 ^[11]	1586 ± 382
F04385-0828 ^[b]	–	2.0	80 ± 14	3 ^[7]	1800 ^[2]	1119 ± 228	F15480-0344 ^[b]	–	2.0	364 ± 53	138 ^[8]	37 ^[13]	< 838
NGC1667 ^[b]	–	2.0	68 ± 11	64 ^[28]	3 ^[29]	76 ± 18	ESO141-G055 ^[b]	?	1.0	107 ± 16	164 ^[8]	2650 ^[50]	–
E33-G2 ^[b,c]	–	2.0	137 ± 20	57 ^[19]	–	–	IRAS19254-7245 ^[a,b]	–	2.0	105 ± 31	602 ^[51]	20 ^[52]	< 323
M-5-13-17 ^[b,c]	–	1.5	98 ± 15	340 ^[19]	–	376 ± 96	NGC6810 ^[b]	–	2.0	68 ± 13	13 ^[7]	–	838 ± 168
IRAS05189-2524 ^[b]	–	2.0	218 ± 16	39 ^[30]	360 ^[31]	2247 ± 451	NGC6860 ^[b,c]	–	1.0	122 ± 18	25 ^[19]	4900 ^[26]	< 2201
Markarian3 ^[c]	1.0	2.0	1763 ± 358	1070 ^[8]	590 ^[32]	1593 ± 349	NGC6890 ^[b]	–	2.0	90 ± 13	72 ^[18]	8 ^[11]	410 ± 97
MRK6 ^[b,c]	–	1.5	385 ± 56	700 ^[8]	1200 ^[33]	–	MRK509 ^[a,b]	–	1.2	286 ± 44	540 ^[8]	5660 ^[53]	1221 ± 254
MRK9 ^[b]	–	1.5	48 ± 8	109 ^[3]	–	< 1944	UGC11630 ^[c]	–	2.0	175 ± 28	–	–	280 ± 77
MRK79 ^[b,c]	–	1.2	395 ± 57	370 ^[3]	2600 ^[15]	< 3567	IC5063 ^[a,b,c]	–	2.0	1139 ± 167	564 ^[8]	1200 ^[29]	2949 ± 598
IRAS07598+6508 ^[a,b]	?	1.0	< 168	–	–	–	UGC11680 ^[b]	–	2.0	45 ± 13	88 ^[54]	–	< 686
MRK622 ^[c]	–	2.0	66 ± 8	40 ^[19]	22 ^[13]	–	PG2130+099 ^[a]	?	1.0	103 ± 16	104 ^[8]	530 ^[55]	861 ± 277
NGC2639 ^[b]	1.4	1.9	36 ± 4	14 ^[34]	25 ^[35]	< 155	IC5135 ^[b]	–	2.0	300 ± 40	27 ^[30]	6 ^[36]	451 ± 90
IRAS08572+3915 ^[a,b]	?	2.0	167 ± 50	8 ^[5]	–	427 ± 85	NGC7172 ^[b]	–	2.0	384 ± 39	10 ^[56]	2200 ^[6]	522 ± 104
MRK704 ^[b]	–	1.5	117 ± 18	85 ^[1]	537 ^[11]	< 10595	IRAS22017+0319 ^[b]	?	2.0	287 ± 42	218 ^[8]	360 ^[57]	–
NGC2841 ^[a]	–	1.0	12 ± 3	–	–	161 ± 51	NGC7213 ^[a,b,c]	–	1.5	45 ± 8	130 ^[8]	3660 ^[14]	798 ± 202
pg0923+129 ^[c]	–	1.2	74 ± 12	90 ^[19]	1151 ^[11]	458 ± 96	3C445 ^[a,b]	–	1.0	71 ± 14	–	700 ^[58]	765 ± 242
UGC5101 ^[a]	3.2	1.5	82 ± 11	21 ^[5]	5 ^[36]	276 ± 55	NGC7314 ^[a,b]	–	1.9	690 ± 101	61 ^[3]	3560 ^[29]	249 ± 65
NGC2992 ^[a,b]	–	1.9	1300 ± 134	360 ^[1]	8030 ^[37]	639 ± 130	UGC12138 ^[a,c]	–	1.8	105 ± 15	144 ^[8]	–	273 ± 57
MRK1239 ^[b]	–	1.5	154 ± 24	467 ^[18]	–	3323 ± 672	M-3-58-7 ^[b]	–	2.0	117 ± 19	251 ^[7]	–	1186 ± 272
NGC3031 ^[a,b]	–	1.8	44 ± 13	100 ^[34]	1500 ^[29]	–	NGC7469 ^[a,b]	–	1.2	322 ± 48	840 ^[1]	2900 ^[49]	2298 ± 460
3C234 ^[b]	?	1.0	79 ± 12	–	–	407 ± 92	NGC7582 ^[a,b]	–	2.0	2449 ± 587	300 ^[1]	1550 ^[29]	309 ± 61
NGC3079 ^[a,b]	2.7	2.0	290 ± 53	945 ^[5]	33 ^[16]	160 ± 32	NGC7590 ^[b]	–	2.0	58 ± 18	11 ^[18]	–	70 ± 17
NGC3227 ^[a,b]	–	1.5	655 ± 95	820 ^[1]	750 ^[38]	–	NGC7603 ^[a,b]	–	1.5	24 ± 4	29 ^[1]	2400 ^[14]	1619 ± 339
NGC3281 ^[c]	–	2.0	1779 ± 534	55 ^[1]	–	162 ± 32	NGC7674 ^[a,b,c]	–	2.0	448 ± 110	718 ^[8]	50 ^[29]	1095 ± 248
NGC3393 ^[c]	2.6	2.0	2214 ± 184	268 ^[18]	9 ^[18]	199 ± 52	NGC7679 ^[a]	–	1.0	350 ± 36	472 ^[5]	458 ^[11]	–
NGC3511 ^[b]	–	1.0	23 ± 6	–	–	27 ± 5	CGCG381-051 ^[b]	–	2.0	< 72	5 ^[8]	–	317 ± 102
NGC3516 ^[a,c]	–	1.5	451 ± 66	270 ^[1]	4410 ^[18]	< 2900	Additional off-sample data						
M+0-29-23 ^[b]	–	2.0	78 ± 23	5 ^[7]	–	348 ± 69	NGC253	–0.8	2.0	1519 ± 239	–	–	–
NGC3660 ^[b]	–	2.0	25 ± 5	33 ^[28]	–	< 234	NGC449	1.7	2.0	–	330 ^[1]	13 ^[13]	–
NGC3783 ^[a,c]	–	1.0	378 ± 57	763 ^[8]	8500 ^[39]	2261 ± 470	NGC591	1.4	2.0	–	1780 ^[3]	18 ^[11]	–
NGC3786 ^[a]	–	1.8	129 ± 19	84 ^[3]	–	281 ± 56	NGC613	1.3	2.0	–	–	–	–
NGC3982 ^[a,b]	–	2.0	89 ± 15	188 ^[34]	22 ^[11]	49 ± 10	IC184	1.4	2.0	–	–	–	–
NGC4051 ^[a,b]	0.3	1.5	366 ± 53	390 ^[34]	627 ^[16]	1704 ± 344	NGC1052	2.1	2.0	–	–	112 ^[36]	–
UGC7064 ^[a,b]	–	1.9	118 ± 17	–	–	269 ± 55	NGC1106	0.9	2.0	–	–	–	–
NGC4151 ^[a,b]	–0.2	1.5	2396 ± 342	11600 ^[34]	4510 ^[16]	7211 ± 1459	MRK1066	1.5	2.0	–	5140 ^[3]	36 ^[13]	–
MRK766 ^[a,b,c]	–	1.0	474 ± 69	453 ^[8]	3000 ^[40]	1061 ± 213	IRAS03355+0104	2.7	2.0	–	76 ^[8]	–	–
NGC4388 ^[a,b,c]	1.1	2.0	2996 ± 644	564 ^[8]	762 ^[16]	971 ± 199	IC342	–2.0	2.0	–	34 ^[59]	–	–
3C273 ^[b]	?	1.0	79 ± 9	116 ^[41]	8300 ^[15]	2043 ± 424	UGC3255	1.2	2.0	–	–	–	–
NGC4501 ^[a,b]	–	2.0	33 ± 6	34 ^[34]	11 ^[16]	< 271	VIIZw73	2.2	2.0	–	74 ^[8]	–	–
NGC4507 ^[a,c]	–	2.0	332 ± 51	828 ^[8]	2100 ^[29]	1579 ± 320	NGC2273	0.8	2.0	187 ± 56	330 ^[3]	69 ^[18]	1014 ± 204
							MRK78	1.5	2.0	792 ± 82	653 ^[60]	–	422 ± 91
							MRK1210	1.9	2.0	209 ± 26	285 ^[18]	840 ^[61]	1244 ± 260
							2MASXJ08362280	3.4	2.0	–	–	–	–

Source	H ₂ O	Sy	[OIV]	[OIII]	2-10 keV	7.6 μ m
NGC2979	2.1	2.0	—	11 ^[18]	—	—
IC2560	2.0	2.0	558 \pm 85	125 ^[18]	39 ^[62]	469 \pm 115
MRK34	3.0	2.0	626 \pm 76	520 ^[1]	35 ^[11]	244 \pm 67
NGC3735	1.3	2.0	—	330 ^[59]	—	—
NGC4258	1.9	1.9	76 \pm 13	100 ^[63]	837 ^[16]	576 \pm 132
ESO269-12	3.0	2.0	—	6 ^[18]	—	—
NGC4945	1.7	2.0	320 \pm 49	—	1300 ^[64]	—
NGC5495	2.3	2.0	—	—	—	—
Circinus	1.3	2.0	8599 \pm 1231	83 ^[65]	1400 ^[66]	39011 \pm 7803
NGC5643	1.4	2.0	940 \pm 142	800 ^[1]	84 ^[18]	—
NGC5728	1.9	1.9	1162 \pm 117	115 ^[18]	133 ^[6]	220 \pm 44
NGC5793	2.0	2.0	—	—	13 ^[11]	—
NGC6240	1.6	2.0	236 \pm 35	202 ^[5]	91 ^[36]	483 \pm 96
NGC6264	3.1	2.0	—	3200 ^[67]	—	—
NGC6323	2.7	2.0	—	—	—	—
NGC6300	0.5	2.0	304 \pm 33	140 ^[68]	860 ^[69]	887 \pm 177
Eso103-G035	2.6	2.0	—	43 ^[18]	907 ^[70]	—
IRAS19370-0131	2.2	2.0	—	—	—	—
NGC6926	2.7	2.0	45 \pm 7	241 ^[5]	—	64 \pm 13
AM2158-380	2.7	2.0	—	—	—	—
NGC7479	1.2	2.0	< 136	—	112 ^[71]	—

Table 3. Measured fluxes and literature values. Column 1: Source names with catalog marks:

a: CfA sample

b: 12 μ m sample

c: IRAS F25/F60 sample

Column 2: Isotropic maser luminosities obtained from Bennert et al. 2009. A question mark designates sources unobserved for masers and a dash represents a maser undetected source.

Note that MRK938 and NGC1320 are listed as Maser in Zhang et al. (2010) but have no luminosity information available. Therefore, they are marked with asterisks. Column 3: Seyfert type obtained from the NED or the literature with references given in square brackets. Column 4: [OIV] flux determined by Ramolla (2009). Column 5: [OIII] flux from the literature. Column 6: 2-10 keV X-ray flux obtained from the literature. Column 7: 7 μ m continuum flux determined by Ramolla (2009). An analysis of the off-sample masers has also been performed. This data is appended in the table.

References:

- 1: Dahari & De Robertis 1988
- 2: Polletta et al. 1996
- 3: Whittle 1992
- 4: Gondoin et al. 2002
- 5: Moustakas & Kennicutt 2006
- 6: Shu et al. 2007
- 7: Tran 2003a
- 8: de Grijp et al. 1992
- 9: Awaki et al. 2000
- 10: Reeves & Turner 2000
- 11: Ueda et al. 2005
- 12: Tran 2003b
- 13: Guainazzi et al. 2005
- 14: Malizia et al. 2007
- 15: Turner & Pounds 1989
- 16: Cappi et al. 2006
- 17: Iyomoto et al. 1996
- 18: Gu et al. 2006
- 19: Schmitt et al. 2003
- 20: Vaceli et al. 1997
- 21: Greenhill et al. 2008
- 22: Véron-Cetty & Véron 2006
- 23: Risaliti et al. 2000

- 24: Bennert et al. 2006
- 25: Boroson & Meyers 1992
- 26: Verrecchia et al. 2007
- 27: Rao et al. 1992
- 28: Storchi-Bergmann et al. 1995
- 29: Bassani et al. 1999
- 30: Kim et al. 1995
- 31: Severgnini et al. 2001
- 32: Bianchi et al. 2005
- 33: Immmler et al. 2003
- 34: Ho et al. 1995
- 35: Terashima et al. 2002
- 36: González-Martín et al. 2006
- 37: Nandra et al. 2007
- 38: Gondoin et al. 2003b
- 39: Blustin et al. 2002
- 40: Matt et al. 2000
- 41: Shang et al. 2007
- 42: Perola et al. 2002
- 43: Miniutti et al. 2007
- 44: Phillips et al. 1983
- 45: Holczer et al. 2007
- 46: Gondoin et al. 2001
- 47: Levenson et al. 2006
- 48: Bianchi et al. 2003
- 49: Reynolds 1997
- 50: Gondoin et al. 2003a
- 51: Buchanan et al. 2006
- 52: Braitto et al. 2003
- 53: Perola et al. 2000
- 54: Kewley et al. 2001
- 55: Lawson & Turner 1997
- 56: Sharples et al. 1984
- 57: Ueno et al. 2000
- 58: Shinozaki et al. 2006
- 59: Ho et al. 1997
- 60: Whittle & Wilson 2004
- 61: Zhang & Fan 2009
- 62: Tilak et al. 2008
- 63: Heckman et al. 1980
- 64: Done et al. 2003
- 65: Oliva et al. 1994
- 66: Smith & Wilson 2001
- 67: Lumsden & Alexander 2001
- 68: Lumsden et al. 2004
- 69: Matsumoto et al. 2004
- 70: Turner et al. 1997
- 71: Panessa et al. 2006